International Journal of Advanced Materials Research
Vol. 2, No. 1, 2016, pp. 1-12
http://www.aiscience.org/journal/ijamr
ISSN: 2381-6805 (Print); ISSN: 2381-6813 (Online)

Ballistic Resistance and Self-Sealing Behavior of Polyhedral Oligomeric Silsesquioxane (POSS)-Enhanced Hydrogenated Nitrile Butadiene Rubber (HNBR) Coating Under High Speed Impact

Liguang Cai*, Ahmed Al-Ostaz, Xiaobing Li, Cole Fowler, Alexander H.-D. Cheng, Hunain Alkhateb

Nano Infrastructure Research Group, Department of Civil Engineering, University of Mississippi, University, USA

Abstract

The ballistic resistance and self-sealing behavior of hydrogenated nitrile butadiene rubber (HNBR) enhanced with polyhedral oligomeric silsesquioxane (POSS) subjected to high speed impact were investigated experimentally and numerically using ANSYS AUTODYN. Both experimental and numerical results showed that the POSS-enhanced HNBR exhibited strong self-sealing properties at both cold temperature and ambient temperature and could dramatically reduce leaking of toxic liquid from a hole in the railcar tank. Close agreements were found between experimental results and simulation results for the ballistic limit of POSS-enhanced HNBR coated and uncoated TC-128 steel plates. Also, the simulation result in terms of the size of hole left in the uncoated TC-128 steel plate was almost the same as the experimental result, while the size of hole left in the POSS-enhanced HNBR coating layer was 155% greater in the simulation result than in the experimental result due to mass erosion. The effects of the thickness of the coating layer on the self-sealing property were also presented in this paper.

Keywords

Impact, Self-sealing, POSS-enhanced HNBR, AUTODYN, TC-128 Steel

Received: December 14, 2015 / Accepted: January 13, 2016 / Published online: January 20, 2016

1. Introduction

Steel railcar tanks provide a promising way to store and transport toxic liquids such as chlorine [1]. However, the release of toxic liquids from holes on the tanks, caused by accidents or high power impacts, is very harmful to the environment and even has deadly impacts on human health [2-4]. So, it is very critical to improve the ballistic resistance of rail tanks with a lightweight polymer coating [5]. Generally, using an elastomer to seal the holes [6] on the tank wall produced by an extremely high speed impact is more effective if the projectile can perforate both the steel tank and protection layer.

Hydrogenated nitrile butadiene rubber (HNBR) is an elastomer used widely as a protection layer for structures under impact loading due to its high damping characteristic [7] and superior impact resistance [8]. When used as a coating layer for a railcar tank containing a toxic liquid, HNBR can largely seal the hole left in the coating layer after impact and significantly decrease the amount of toxic liquid leaking from the hole. HNBR can perform both solid and liquid behaviors at certain temperatures [9]. When the operating temperature is greater than the glass transition temperature, HNBR can stretch to several times longer than its initial length under loading and then almost return to its original dimension under unloading [10]. In this case, the

* Corresponding author
E-mail address: lcai3699618@gmail.com (Liguang Cai)

local motion of the HNBR molecular segment is like liquid flowing, although the HNBR is still solid at the macro level. The self-sealing property of HNBR is mainly due to its liquid-like property. Self-sealing provides a costless method for repairing the micro cracks in an object that are caused by thermal fatigue and the holes generated by external high speed impacts [11]. Some composite materials without self-sealing properties, adding healing agents [12-16] can also effectively seal the cracked, damaged area and restore the fracture toughness.

There are extensive studies on the low speed impact of rubber projectiles on various materials using different software such as LS-DYNA and ABAQUS [17-21]. In these studies, the –Mooney-Rivlin material model [22] was used for rubber materials. More recently, the shape-charged jet impact on rubber composites has been studied extensively [23-25]. It is found that Kevlar woven fabric is an effective reinforcement for rubber composite armor, since Kevlar can significantly reduce the penetrative ability and disturb the moving jet [23]. In this paper, the self-sealing behavior of a polyhedral oligomeric silsesquioxane (POSS)-enhanced HNBR coated TC-128 steel plate under high speed impact was investigated experimentally and numerically. For the numerical simulation, ANSYS AUTODYN was used and the Ogden 3rd order material model [26] was applied for the POSS-enhanced HNBR since this model can be applied to materials that have a yield strain up to 700% [27]. For the comparison, the ballistic test and numerical simulation results for the uncoated steel plates were also presented in this paper.

2. Experimental

2.1. Materials

In this study, all unvulcanized HNBR raw rubber materials were purchased from Zeon Chemicals L.P., Louisville, KY, USA. HNBR, made from the mixture of Zetpol 2020/ZSC 2295 CX (35/65 by weight), has outstanding tensile, tear and abrasion properties. The TC-128 steel plates used in the ballistic test were purchased from Clifton Steel Company, Maple Heights, OH, USA.

Polyhedral Oligomeric Silsesquioxane (POSS) is a class of silicon based nano chemicals designed to fulfill various mechanical functions. In this study, TriSilanolIsooctyl (TSS, product number: SO1455) POSS and TriSilanolPhenyl (TSP, product number: SO1458) POSS were added to the HNBR for the investigation. The POSS compounds were purchased from Hybrid Plastics Inc., a Hattiesburg, MS, USA.

The unvulcanized HNBR materials are viscous materials similar to gum. They can only be processed in heavy-duty steel molds that must be clamped under very high tonnage during molding. Manville Rubber Products, Inc., Manville, NJ, USA, carried out the mixing and vulcanization (curing) of all HNBR samples. Table 1 summarizes the formulations for HNBR. Square sheets of HNBR (300 mm × 300 mm × 1.6 mm) are used for the characterization of the mechanical properties contained POSS loading of 0, 1, 2, 3, 4, or 5 phr (The unit phr denotes parts per hundred rubber.). The uncured HNBR raw materials, additives (Table 1) and specific amounts of POSS were mixed by the Banbury mixer. The mixture was then cured in a mold at 165.6°C for 30 min. The POSS-filled HNBR (POSS loading of 3 phr) that coated the steel plate for the ballistic test was mixed the same way. The mixture was applied to the entire surface of the square steel sheet (300 mm × 300 mm) in the mold and then cured at 165.6°C for 60 minutes. The thickness of the HNBR/POSS (3phr) coating layer was controlled to be 38.1 mm.

Table 1. Formulations of HNBR.

Formulation of Pure HNBR	
Zetpol 2020/ZSC 2295 CX (35/65 by weight)	
3 phr	N110 carbon black
0.5 phr	Agerite Resin D antioxidant
9.375 phr	Varox DCP-40KE
1 phr	Agerite Resin D
3 phr	N-550
0.5 phr	HVA-2
3 phr	Di-Cup 40KE

2.2. Tensile Test

2.2.1. Test Description

Tensile tests were performed for the TSP or TSS POSS enhanced HNBR using an Instron 5982 dual column floor model test system at room temperature, as shown in Fig. 1. The goal of static mechanical evaluation was to determine the effect of adding nano materials on the improvement of the mechanical properties of the polymers used. It is essential to identify the ideal phr of POSS materials that gave the base polymer the greatest improvement in physical properties.

(a)

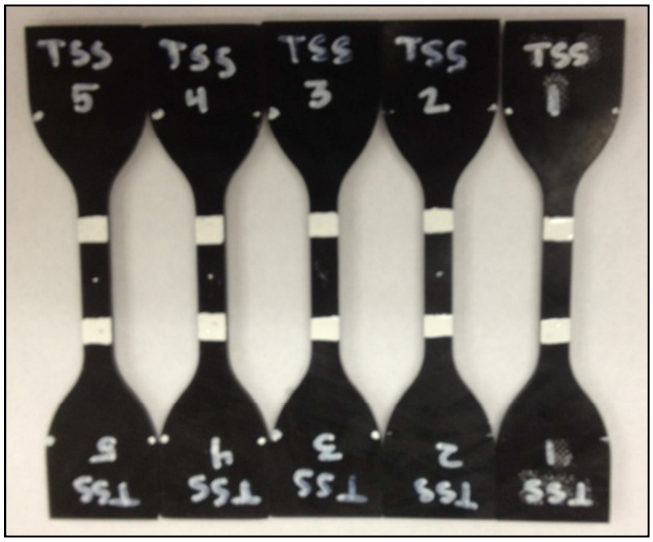

(b)

Fig. 1. (a) Instron 5982 dual column floor model test system (b) HNBR samples with different phr of TSS POSS shown with paint marks.

Testing of hyperelastic materials can be difficult due to their excessive extension capacity. The gauge section of a test specimen will stretch along with portions of the grip sections, causing error in the strain calculation. This effect was combated by the use of a video extensometer. The video extensometer shown in Fig. 1 was mounted on an Instron 5982 dual column floor model test system. Two paint marks on each specimen's gauge length allowed the camera to pick up movement of the preset points using contrast. Data captured from the video provided a relative gauge length measurement regardless of the absolute movement of the grips. Another issue with hyperelastic materials is the Poisson's effect at the grip surface, which can cause slippage. This effect was combated with the use of pneumatic grips that supplied a constant pressure along the grip surface throughout the test.

Testing for each material was comprised of at least five specimens per sample. Stress-strain curves were recorded in real time, and, depending on the data, more specimens were tested if needed. Each specimen was secured with grips set at approximately 207-241 kPa.

2.2.2. Tensile Test Results and Discussion

The true stress-strain curve, ultimate true stress and strain of HNBR with different phr of TSS and TSP POSS are plotted in Fig. 2 (a)~(d). Compared with pure HNBR, HNBRs with varied phr of TSS or TSP POSS have smaller ultimate yield stresses. There was a distinct increase of elongation as the amount of TSS and TSP POSS increased to 3phr, and then there is a drop off in performance when the amount of TSS and TSP POSS continued increasing. Therefore, the tensile test performance of HNBR with different phr of TSS and TSP POSS was highly dependent on the amount of POSS. The HNBR/3phr TSS POSS and HNBR/3phr TSP POSS, which have highest material properties among the tested materials, were used as the coating layer for the TC-128 steel plates.

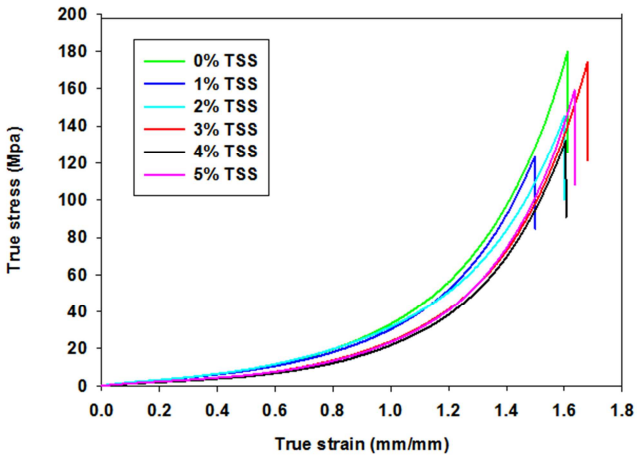

(a)

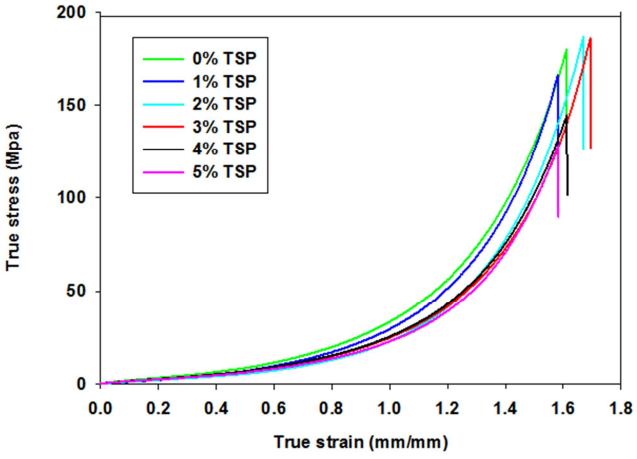

(b)

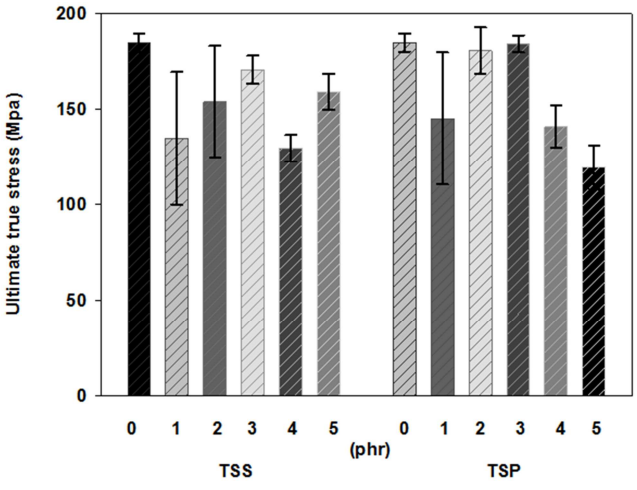

(c)

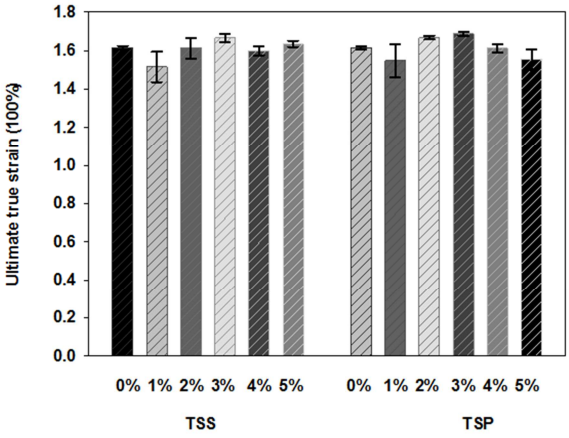

(d)

Fig. 错误!文档中没有指定样式的文字。**.** (a) True stress-strain curve for HNBR with different phr of TSS POSS. (b) True stress-strain curve for HNBR with different phr of TSP POSS. (c) Ultimate true stress for HNBR with different phr of TSS and TSP POSS. (d) Ultimate true strain for HNBR with different phr of TSS and TSP POSS.

2.3. Ballistic Limit Test

2.3.1. Ballistic Limit Test Description

The ballistic limit test was performed at H.P. White Ballistic Laboratory in Street, MD, USA. During the test, a standard 0.50 caliber M33 ball as shown in Fig. 3 was shot into the plates which were mounted on a rigid support structure. The parameters of 0.50 caliber M33 ball round were tabulated in Table 2. Fig. 4 shows the experimental set-up of ballistic limit test. The target plates were secured to a floor-mounted heavy steel rack 7.6 meters from the test barrel. The plates were secured to the rack by C-clamps. A laser levelling device was used to align each shot. Two photoelectric infrared screens, placed three and six meters forward from the barrel, were used in conjunction with a chronograph in order to calculate the average velocity of the projectiles. The velocities were manipulated by increasing or decreasing the amount of propellant used in each cartridge.

Fig. 3. 0.50 caliber M33 ball round.

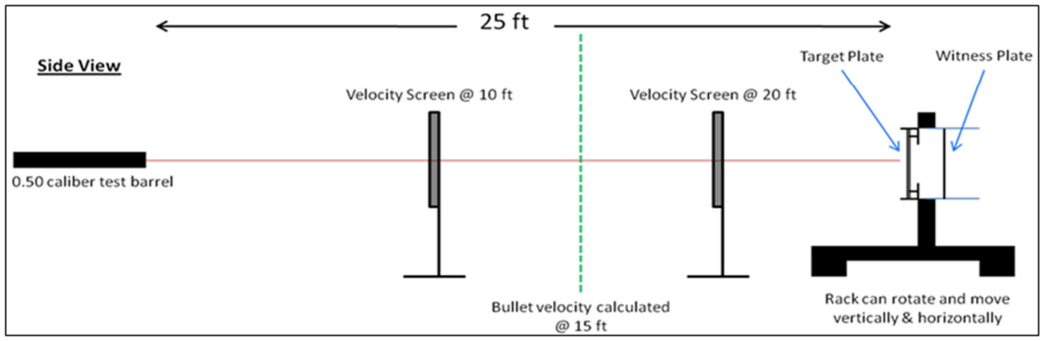

Fig. 4. Experimental set-up of ballistic limit test.

Fig. 5 shows a 0.50 mm thick sheet of 2024-T3 aluminum which was used as a witness plate to determine partial or complete penetration. At least three shots had to penetrate and three had to not penetrate to get the ballistic limit of plates. So, the plates were shot multiple times, until sufficient data was gathered to quantify an accurate ballistic limit. After the test, the sizes of the holes produced by the impacts were measured.

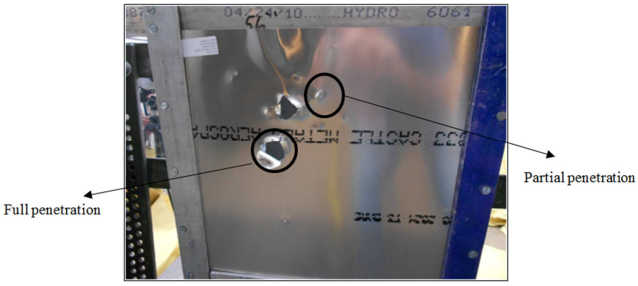

Fig. 5. Aluminum witness plate shown after full penetration of steel target plate and partial penetrations around the main crater.

Table 2. Parameters of 0.50 caliber M33 ball round.

Diameter (mm)	Length (mm)	Projectile weight (g)	Velocity (m/s)
12.7	138.4	42.96	914

Fig. 6 shows the configurations of HNBR/3phr TSS POSS or HNBR/3phr TSP POSS coated and uncoated TC-128 steel plates for the ballistic limit tests. An HNBR/3phr TSS POSS layer or an HNBR/3phr TSP POSS layer was placed in front of the TC-128 steel plate in order to seal the hole produced by the bullet impact. The areas of the HNBR/3phr TSS POSS and HNBR/3phr TSP POSS TC-128 steel layers are both 300 mm × 300 mm. The thicknesses of the HNBR/3phr TSS POSS, HNBR/3phr TSP POSS and TC-128 steel plate layers are 38.1 mm, 38.1 mm and 19.05 mm, respectively.

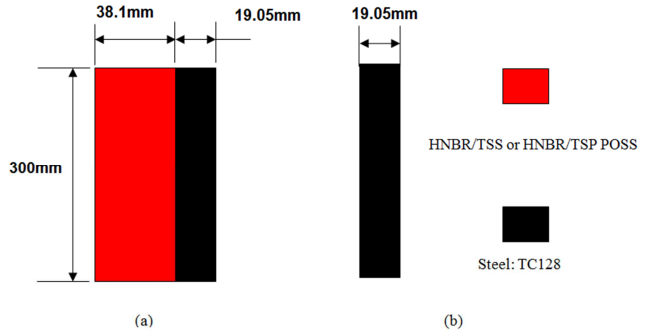

Fig. 6. Configuration of (a) HNBR/3phr TSS POSS coated (in front) (b) uncoated steel plates for the ballistic limit test.

A supplemental test was administered after the initial ballistic limit experiments. Many tankers may carry compressed chlorine gas, which exists at a sub-zero temperature in liquid form. The idea was to have a small-scale study of the effect of extreme cold on the impact mechanics of the plate and the behavior of the coatings. Two plates, one coated with HNBR/3phr TSS POSS and one with HNBR/3phr TSP POSS, were conditioned at -34.4°C for 24 hours and then subjected to the previously mentioned ballistic limit tests.

2.3.2. Ballistic Limit Test Results and Discussion

The ballistic test results for the HNBR/3phr TSS POSS, HNBR/3phr TSP POSS coated and uncoated TC-128 steel plates are summarized in Table 3. The ballistic limits for the HNBR/3phr TSS POSS coated and uncoated TC-128 steel plates were 1015 m/s and 971 m/s, respectively. The HNBR/3phr TSP POSS coated TC-128 steel plate completely resisted all shots and there were no ballistic limit measurements. Also, the highest partial penetration velocity for HNBR/3phr TSP POSS coated TC-128 steel plate was 1023 m/s, which indicated that the HNBR/3phr TSP POSS coated TC-128 steel plate had the best ballistic resistance performance due to the better mechanical properties of the coating material. Considering the weight added to the steel railcar tank, HNBR/3phr TSS POSS did not have a significant effect (by 4.5 percent of increment) on the ballistic resistance of the TC-128 steel substrates. Although Roland et al. [28] found that the front-surface polyurea or nitrile rubber (NBR) layers can significantly increase the ballistic limit of high hard steel (HHS), the limited improvement of ballistic limit of TC-128 steel substrates in our study may be due to the lower hardness of TC-128 steel compared to the HHS. Our prior study also showed that the polyurea/3phr TSS POSS coating can not increase the ballistic resistance of TC-128 at all [29].

Table 3. Ballistic test results for HNBR/3phr TSS POSS coated and uncoated steel plate.

Configuration	Shot	Velocity (m/s)	Result	Include	V-50 (m/s)	Range
Uncoated steel plate	1	927.5	P	N	971.1	8.8
	2	928.1	P	N		
	3	NR	C	N		
	4	970.8	C	Y		
	5	967.4	P	Y		
	6	976.3	C	Y		
	7	969.6	P	Y		
HNBR/3phr TSS POSS coated steel plate	1	1007.7	P	N	1015	8.2
	2	1012.2	P	Y		
	3	1013.8	P	Y		
	4	1013.8	C	Y		
	5	1014.4	P	Y		
	6	1015.3	C	Y		
	7	1020.5	C	Y		
HNBR/3phr TSP POSS coated steel plate	1	1015.3	P	N	1023^{+}	N
	2	1014.4	P	N		
	3	1023.5	P	N		

V-50: Ballistic limit P: Partial penetration; C: Complete penetration; Y: Included for V-50 calculation; N: Not included for V-50 calculation; 1023^{+}: Greater than 1023.

Fig. 7 (a)-(i) shows the HNBR/3phr TSP POSS, HNBR/3phr TSS POSS coated and uncoated TC-128 steel plates at and after impact. As shown in the Fig 7 (b), the HNBR/3phr TSP POSS coating layer was stretched significantly during impact. The size of the hole in the HNBR/3phr TSP POSS coating layer increased to its maximum value first and then decreased during impact. The high speed impact also caused a large amount of mass loss of HNBR/3phr TSP POSS and HNBR/3phr TSS POSS coating layer, as shown in Fig. 7 (c)~(d). Even so, The size of the hole left in both HNBR/3phr TSP POSS and HNBR/3phr TSS POSS coating layer after impact was 3.5 mm in diameter (Fig. 7(e)~(f)), while the hole in the uncoated steel plate remained about 15 mm in diameter as shown in Figure 7(g). As shown in Fig. 7(e)~(f), the two coating materials exhibit “brittle” failure mode after impact, which is due to a transition of the coating layer from "rubbery" state to "glassy" state induced by the high speed impact [28].

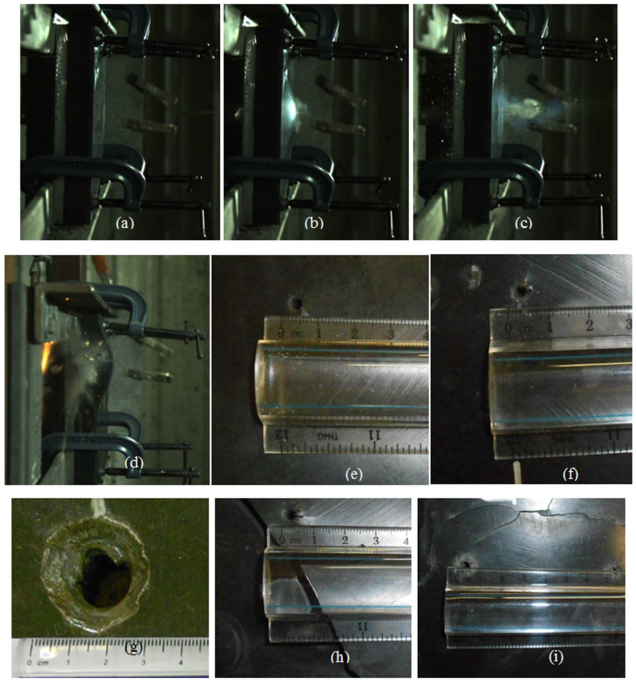

Fig. 7. (a) Side view of initial impact of HNBR/3phr TSP POSS coated TC-128 steel plates before impact. (b) Side view of HNBR/3phr TSP POSS coated TC-128 steel plates at maximum deflection during impact. (c) After penetration, large amount of HNBR/3phr TSP POSS is lost. (d) After penetration, large amount of HNBR/3phr TSS POSS is lost. (e) The coated HNBR/3phr TSP POSS closed to the minimal hole after impact. (f) The coated HNBR/3phr TSS POSS closed to the minimal hole after impact. (g) Hole left in the front side of uncoated steel layer after impact. (h) Hole left in the HNBR/3phr TSP POSS coated TC-128 steel plate with cracks after cold testing. (i) Hole left in the HNBR/3phr TSS POSS coated TC-128 steel plate with cracks after cold testing.

At cold temperature, the plates tested were not penetrated due to excessive barrel pressure. Since there was no penetration, there could be no ballistic limit measurement; however, the high partial penetration velocities for the HNBR/3phr TSP POSS and HNBR/3phr TSS POSS coated TC-128 steel plate were both 1017 m/s. Fig. 7 (h)~(i) shows the HNBR/3phr TSP POSS and HNBR/3phr TSS POSS coated TC-128 steel plate after cold testing. The coatings layers lost much of their elastic behavior at low temperature and showed signs of brittle fracture. During impact, the size of the hole in both coating layers increased first and then decreased. The craters left in both of the two coating layers were 4 mm in diameter. So, at low temperature, the coating materials showed brittle behavior but did not lose the self-sealing and ballistic resistance improvement ability, suggesting that both HNBR/3phr TSP POSS and HNBR/3phr TSS POSS would be an effective protection layer for steel railcar tanks carrying compressed toxic gas, which exists at a sub-zero temperature in liquid form.

Hyperelastic materials respond elastically even when subjected to very large strains. There is no plastic strain remained under unloading condition after impact. Ideally, the hole should be completely closed after impact. However, both coating layers did not completely self-seal the holes after impact. The primary reason is the mass loss of coating material during impact, as shown in Fig. 7 (c), which might be due to a small shear plug formed at the bullet tip of impact site [30, 31]. Therefore, a thicker layer of coated elastomer will be desirable to accommodate the mass loss and ensure the remaining mass of elastomer is enough to seal the cut-through hole completely. Moreover, the "brittle" failure of coating layer induced by high speed impact could also increase the mass loss of coating layers. Therefore, the effectiveness of self-sealing of coating layer highly depends on the thickness of elastomer coating layer, the diameter of projectile and the impact velocity. Indeed, in another experiment, we found that a layer of polyurea/POSS rubber (4-6 mm thick) completely sealed the hole generated by a smaller projectile (~4.5 mm in diameter) at a low speed of 200 m/s, regardless complete or partial penetration.

3. Finite Element Analysis

3.1. Material Model

3.1.1. Projectile

The two main components of the projectile are a copper jacket and a steel core. During the test, the copper jacket was totally ripped off. This happened because the strength of the copper jacket is so small compared to that of the TC-128 steel plate. In addition, Børvik et al [32] found that the brass jacket, which has a much higher strength than the copper jacket, has almost no influence on the ballistic limit of steel targets. So, for all the simulations, the steel core was used to represent the whole projectile.

The equation of state (EOS) of the steel core is linear and defined as:

$$P = ku \tag{1}$$

Where k is the material bulk modulus, and u is the specific volume.

For the strength model, the material properties of the steel core are still uncertain because the required test data are generally not available in the literature. The Rockwell C hardness (HRC) value of the steel core, which is the only known parameter, is equal to 53 and was provided by the H.P White Company. So, the tensile test data of Arne tool steel with an HRC value equal to 53 was used for the steel core [33]. The bilinear hardening strength model was used to fit the experimental data. The expression of the bilinear hardening strength model is,

$$\sigma = \begin{cases} E\varepsilon & \varepsilon \le \varepsilon_0 \\ \sigma_0 + E_t(\varepsilon - \varepsilon_0) & \varepsilon > \varepsilon_0 \end{cases} \tag{2}$$

Where E is Young's modulus and E_t is the tangent modulus.

The failure model for the projectile was not considered at this stage, but the erosion technique was used to represent the failure of the projectile material. This element is deleted from further calculation if the effective plastic strain (EPS) in that element reached a value of 1. The model constants for the projectile are reported in Table 4.

Table 4. Model constants for projectile.

Equation of State				Strength Model			Erosion
ρ(g/cm^3)	K (GPa)	T_0(k)	C_p (j/(kg. K))	G (GPa)	σ_o (MPa)	E_t(GPa)	EPS
7.75	200	300	477	76.69	1,900	15,000	1

3.1.2. TC-128 Steel Plates

The EOS of TC-128 steel can also be described by (1), which only needs one parameter.

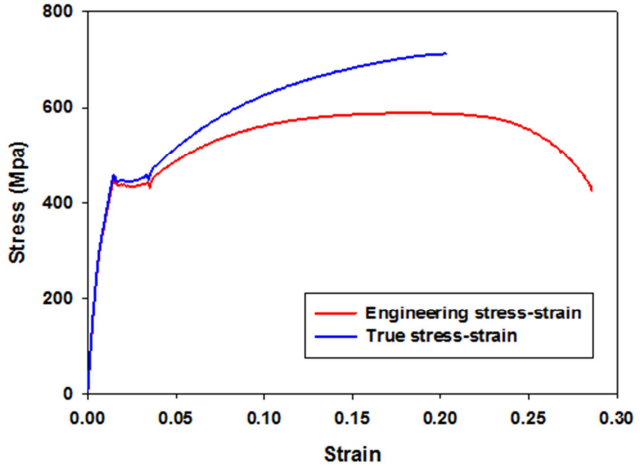

Fig. 8. True and engineering stress-strain curve of TC-128 steel.

For the strength model, the quasi-static tensile test was performed for the TC-128 steel plate at room temperature and at a strain rate of 5.10^{-4} s^{-1}. The engineering strain-stress curve and true strain-stress curve were plotted in Fig. 8. The piecewise model, a modification model to the Johnson-Cook model, was used as the strength model for the TC-128 steel plate. For the Johnson-Cook model (JC model), the stress can be expressed as a function of strain, strain rate and temperature, i.e.:

$$\sigma = \left[A + B\varepsilon_{pl}^{n}\right]\left[1 + Cln\dot{\varepsilon}_{pl}\right]\left[1 - T_{H0}^{m}\right] \quad (3)$$

Where ε_{pl} is the equivalent plastic strain, $\dot{\varepsilon}_{pl}$ the equivalent plastic strain rate, A, B, and C are material parameters (A is the initial yield stress, B is the hardening constant, and C is the strain rate constant), n and m are the hardening exponent and thermal softening exponent respectively, and $T_{H0} = (T - T_{room})/(T_{melt} - T_{room})$ and is the nondimentional normalized (homologous) temperature (room temperature is T_{room} and T_{melt} is the melting temperature).

For the piecewise model, the strain rate hardening and thermal softening parts are the same as in the JC model while the strain hardening part $\left[A + B\varepsilon_{pl}^{n}\right]$ in JC model is replaced by a piecewise linear function of yield stress versus effective plastic strain. In AUTODYN software, the strain hardening part of the piecewise model can be obtained with up to ten EPS and yield stress (YS) data points. For the strain rate constant C and thermal softening exponent m, the parameters of weldox 460 E steel ,which has almost the same yield strength and ultimate strength as TC-128 steel, are used here [34].

The failure model of TC-128 steel is based on the EPS value. When the EPS exceeds 1, element failure occurs. The model constants for the TC-128 steel plate are summarized in Table 5.

Table 5. Model constants for TC-128 steel.

Equation of State				Failure model
ρ(g/cm^3)	K (GPa)	T_0(k)	C_p (j/(kg. K))	EPS
7.98	181	300	455	1

Strength Model							
G (GPa)	σ_o (MPa)	EPS 1~6					
76	455	0.0004	0.0057	0.03	0.1	0.17	0.2

Strength Model									Failure model
ES 1~6 (MPa)						C	m	T_m(°k)	EPS
448	446	506	646	704	707	0.006	0.893	1800	1

3.1.3. HNBR/3phr TSS POSS

The numerical simulation is limited to the HNBR/3phr TSS POSS coated and uncoated TC-128 steel plate subjected to impact at ambient temperature. It assumes here that the material properties of the base material of the HNBR/3phr TSS POSS layer and the bond between the HNBR/3phr TSS POSS and the steel plate are the same [31]. So, the following material models and model constants are applied for both materials.

A hyperelastic equation of state is used for HNBR/3phr TSS POSS. Specific heat and thermal conductivity are the two parameters needed to be defined for this EOS. Currently, the hyperelastic EOS can be used in Lagrange unstructured solver, in which the thermal conductivity had been set to 0. The specific heat of HNBR/3phr TSS POSS at 293k was set as 2410 j/(kg. K) [35].

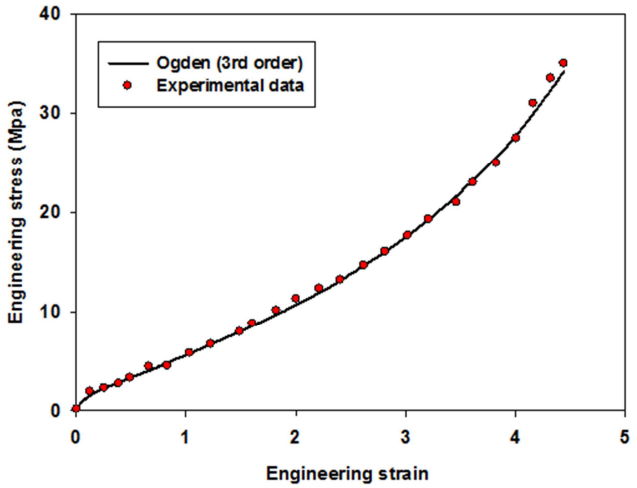

Fig. 9. Curve fitting for experimental data of HNBR/3phr TSS POSS using Ogden 3rd order.

Fig. 9 plots the engineering stress-strain curve of HNBR/3phr TSS POSS fitted by an Ogden 3rd order and it shows that the model fits the experimental data quite well. The strain energy function for this hyperelastic strength model is defined as

$$\varphi=\frac{\mu_1}{\alpha_1}(\overline{\lambda_1^{\alpha_1}}+\overline{\lambda_2^{\alpha_1}}+\overline{\lambda_2^{\alpha_1}}-3)+\frac{\mu_2}{\alpha_2}(\overline{\lambda_1^{\alpha_2}}+\overline{\lambda_2^{\alpha_2}}+\overline{\lambda_2^{\alpha 2}}-3)$$
$$+\frac{\mu_3}{\alpha_3}(\overline{\lambda_1^{\alpha_3}}+\overline{\lambda_2^{\alpha_3}}+\overline{\lambda_2^{\alpha_3}}-3)+\frac{1}{d_1}(J-1)^2+\frac{1}{d_2}(J-1)^4+\frac{1}{d_3}(J-1)^6 \quad (4)$$

Where λp is Deviatoric principal stretches of the left Cauchy-Green tensor, J is determinant of the elastic deformation gradient, μ_p α_p and d_p are material constants (Here, p=1, 2, 3)

Principal tensile failure strain (PTFS) was applied as the failure criterion for HNBR/3phr TSS POSS. If the values of PTFS in the element reach 4.44, then the element cannot sustain any tensile stress. The model constants for HNBR/3phr TSS POSS are reported in Table 6.

Table 6. Model constants for HNBR/3phr TSS POSS.

Equation of State			**Failure model**
ρ(g/cm^3)	**T_0(k)**	**C_p (j/(kg. K))**	**PTFS**
1.05	293	2410	4.44

Strength Model								
μ_1 (Kpa)	**α_1**	**d_1 (/Kpa)**	**μ_2 (Kpa)**	**α_2**	**d_2 (/kpa)**	**μ_3 (Kpa)**	**α_3**	**d_3(/kpa)**
426.12	3.52	1.04e-7	12909.88	0.236	0	12944.14	0.241	0

3.2. Model Architecture

Fig. 10 shows the configuration of the HNBR/3phr TSS POSS coated and uncoated TC-128 steel plates built in AUTODYN. Lagrange solvers were used to represent the bullet and HNBR/3phr TSS POSS, and the numbers the elements of the bullet and HNBR/3phr TSS POSS elements are 2032 and 28800, respectfully. The TC-128 steel was represented by 14400 particles using smoothed-particle hydrodynamics (SPH) solver. Interaction between different layers is modeled with a Largrange-Lagrange interaction. The dimensions of TC-128 steel and coating layer are 300 mm long × 300 mm wide for the model. A fixed boundary condition was applied at the top and bottom edge of steel and coating layer. The impact velocity of bullet was increased from 800 m/s to 1000 m/s to determine the ballistic limit of PU/3phr epoxy POSS coated and uncoated steel plate. Geometry strain is used as the erosion criteria and 3 is the erosion limit for the HNBR/3phr TSS POSS. The element is deleted from further calculation if the geometry strain in that element reaches 3.

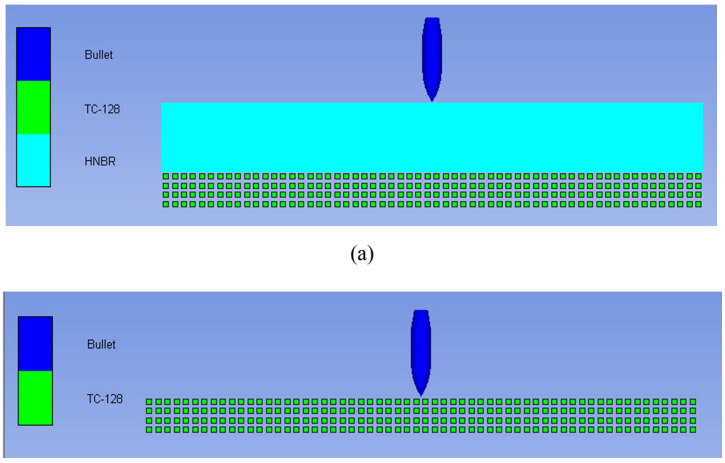

Fig. 10. Configuration of (a) HNBR/3phr TSS POSS coated (b) uncoated TC-128 steel plate built in AUTODYN.

3.3. Result and Discussion

3.3.1. Comparison between the Experimental and Simulation Results

The numerical results in terms of ballistic limits of HNBR/3phr TSS POSS coated and uncoated TC-128 steel plates subjected to high speed impact are reported in Table 7. The average value of the minimum full penetration velocity and maximum partial penetration velocity is considered as the ballistic limit. For HNBR/3phr TSS POSS coated and uncoated TC-128 steel plates, the ballistic limits are 875 m/s and 955 m/s respectively. So, as shown by the experimental results, the HNBR/3phr TSS POSS coating can increase the ballistic limit of a TC-128 steel plate without adding much weight. Fig. 11 shows a comparison of the experimental and numerical results of the ballistic limit. The numerical simulation results agree quite well with the experimental results and the average error is about 7.75%.

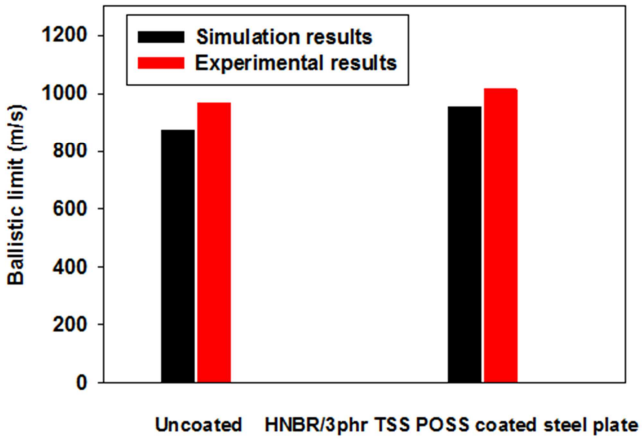

Fig. 11. Comparison of the experimental and simulation results of the ballistic limit.

Table 7. Numerical results in terms of the ballistic limit of HNBR/3phr TSS POSS coated and uncoated TC-128 under high power impact.

Configuration	Impact velocity (m/s)	Result	Residual velocity (m/s)	V_{50} (m/s)
Uncoated steel plate	860	P	0	875
	870	P	0	
	880	C	49.3	
HNBR/3phr TSS POSS coated steel plate	950	P	0	955
	960	C	30.39	
	970	C	64.1	

P: Partial penetration; C: Complete penetration; V_{50}: Ballistic limit.

Fig. 12 shows a snapshot of the uncoated and HNBR/3phr TSS POSS coated TC-128 steel plates impacted at a velocity equal to 1000 m/s. For the uncoated steel plate, the hole size increased from 0 to 15.1 mm and then remained constant while the size of the hole left in the HNBR/3phr TSS POSS layer increased from 0 to 26.9 mm and then decreased to 8.9 mm. So, the HNBR/3phr TSS POSS coating layer exhibited self-sealing properties.

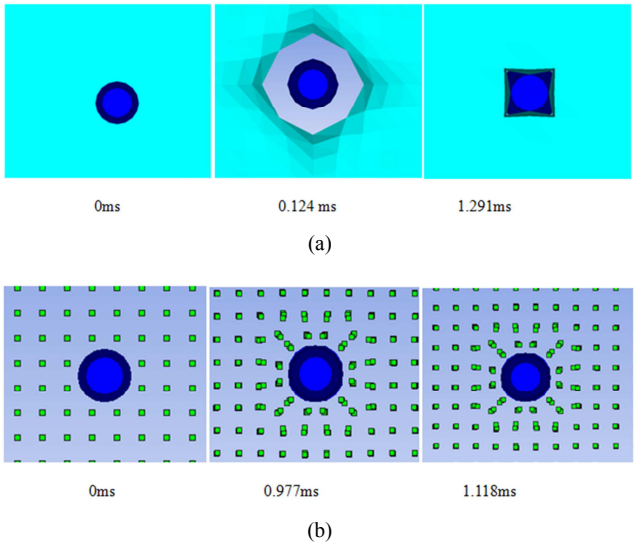

Fig. 12. The snapshot of (a) HNBR/3phr TSS POSS coated (b) uncoated steel plate impacted at a velocity of1000 m/s.

Fig. 13 compares the experimental and simulation results in terms the size of hole left in the uncoated TC-128 steel plate and HNBR/3phr TSS POSS coating layer. It shows that the simulation results for the uncoated TC-128 steel plate are almost the same as the experimental results while the simulation results for the HNBR/3phr TSS POSS coating layer are about 155% higher than the experimental results.

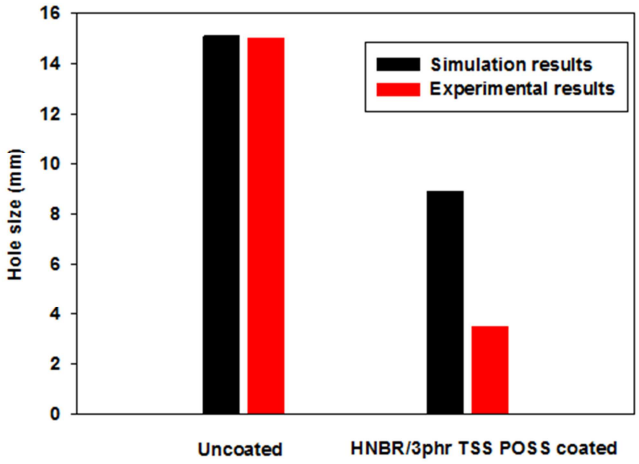

Fig. 13. Comparison of hole size between experimental and simulation results.

The overestimation of the size of the hole left in the HNBR/3phr TSS POSS coating layer is due to the mass loss

which is caused by element erosion. Fig. 14 plots the mass time history for the coating layer, and it shows that the mass of the coating layer decreased about 0.1% because of mass erosion. However, the mass of the TC-128 steel plate keep the same when using the SPH solver, which is a mesh-less technique for which no erosion technique is needed for a large deformation simulation such as a simulation for a high speed or even a hypervelocity impact physical event [36]. So, mass erosion is the reason why the simulation results in terms of the size of the hole left in the HNBR/3phr TSS POSS coating layer are much higher than the experimental results while the size of the hole in the uncoated TC-128 steel plate is the same as in the experimental results.

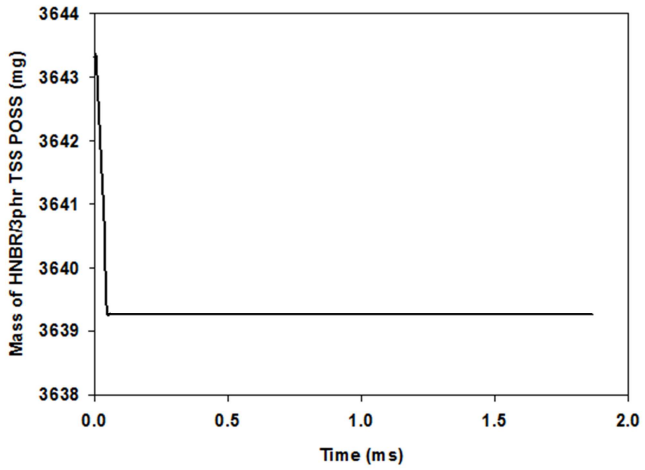

Fig. 14. Mass time history for the HNBR/3phr TSS POSS coating layer.

3.3.2. Parameter Evaluation

i. Erosion limit

The erosion, a nonphysical-based phenomenon, is used to remove the severely crushed element in the Lagrange solver, which leads to the numerical stability. On one hand, it is necessary to increase the erosion limit of HNBR/3phr TSS POSS so that the elements do not "erode" until they are severely deformed, which will decrease the mass loss due to erosion and make the simulation results in terms of the hole size closer to the experimental results. On the other hand, a higher erosion limit always causes extreme computational inefficiency [37]. Fig. 15 displays the mass of the HNBR/3phr TSS POSS coating layer which is 38.1 mm thick before and after erosion for different erosion limits. It shows that increasing the criteria limit from 3 to 30 does not result in the decrease of the mass loss of the coating layer due to erosion. So, an erosion limit of 3 is reasonable and is used for the following simulation for computational efficiency.

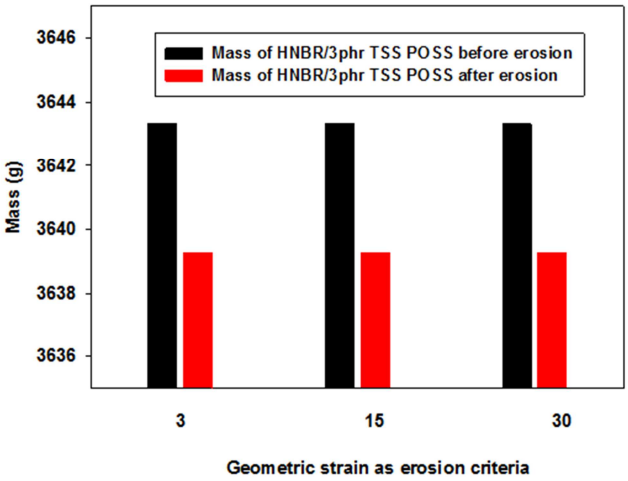

Fig. 15. The mass of HNBR/3phr TSS POSS coating layer before and after erosion at different geometric strain as erosion criteria.

ii. Thickness

A series of simulations have been conducted for the HNBR/3phr TSS POSS coated steel plate impacted at a velocity equal to 1100 m/s and with the thickness of the coating layer increased from 5 mm to 40 mm. Fig. 16 plots the hole size after impact in coating layers with different thicknesses. The size of the hole in the coating layer decreased sharply when the thickness of the coating layer increased from 5 mm to 10 mm and decreased slightly when the thickness increased from 10 mm to 40 mm. Therefore, the thickness of the coating layer is a very critical parameter for the self-sealing properties. Compared with uncoated steel plate, coating layer almost did not decrease the hole size if its thickness is less than 5 mm.

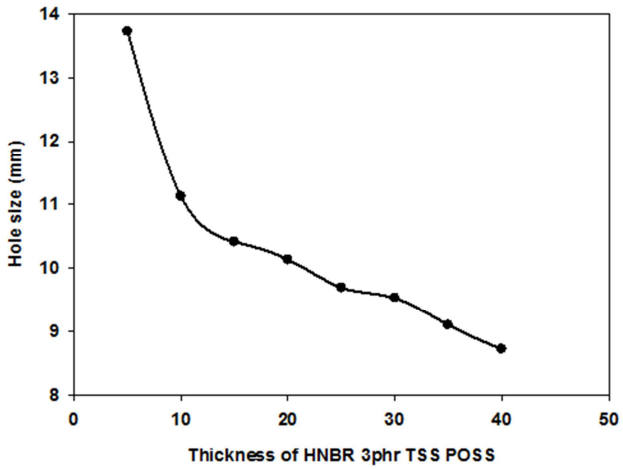

Fig. 16. The hole size of HNBR/3phr TSS POSS coating layer as function of its thickness.

4. Conclusion

In this paper, the experimental tests and numerical simulations were performed to study the self-sealing

behavior of HNBR/3phr TSP POSS and HNBR/3phr TSS POSS coating layers subjected to high speed impact. The experimental results showed that the size of the hole left in both HNBR/3phr TSP POSS and HNBR/3phr TSS POSS coating layers was only 3.5 mm, while the hole size was 15 mm for the uncoated TC-128 steel plate after impact. So, the coating layer exhibits a strong self-sealing property under high speed impact. The coating layer can increase the ballistic limit of TC-128 steel plates, which was also shown in the experimental results. The cold testing results showed that the coating materials did not lose the self-sealing and ballistic resistance improvement ability at low temperature even with brittle behavior.

Numerical simulations of the impact of a standard 0.50 caliber M33 ball on HNBR/3phr TSS POSS coated and non-coated TC-128 steel plates were conducted using AUTODYN. Close agreements were found between the experimental results and simulation results for the ballistic limit of coated and uncoated TC-128 steel plates and the average error was 7.75%. Also, simulation results in terms of the size of the hole left in uncoated TC-128 steel plates were almost the same as the experimental results, while the size of the hole left in the coating layer was 155% greater than in the experimental results due to mass erosion. The simulation results also show that the increase in the thickness of the coating layer results in a reduction in the size of the hole left in the coating layer.

Acknowledgements

Authors acknowledge the financial support received under a subcontract from the Department of Homeland Security-sponsored Southeast Region Research Initiative (SERRI) at the Department of Energy's Oak Ridge National Laboratory for this research work (Basic Agreement number 4200000224).

References

[1] Ale. BJM, Golbach G., Goos D., Ham K., Janssen L. Shield S. Benchmark Risk Analysis Models, RIVM report 6100066015, Bithoven, The Netherlands, 2001, 1-48.

[2] Hanna S, Dharmavaram S, Zhang J, Sykes I, Witlox H, Khajehnajafi S, et al. Comparison of six widely-used dense gas dispersion models for three recent chlorine railcar accidents. Process Safety Progress 2008; 27:248-59.

[3] Saat MR, Barkan CPL. The Effect of Rerouting and Tank Car Safety Design on the Risk of Rail Transport of Hazardous Materials, in: Proceedings of 7th World Congress on Railway Research, Montreal, Quebec, Canada, 2006.

[4] Hanna SR, Hansen OR, Ichard M, Strimaitis D. CFD model simulation of dispersion from chlorine railcar releases in industrial and urban areas. Atmospheric Environment 2009; 43:262-70.

[5] Fowler MC. Experimental and numerical analysis of nano-enhanced polymer coated steel plates subjected to ballistic loading. Thesis,The University of Mississippi, 2012.

[6] Persson B, Albohr O, Tartaglino U, Volokitin A, Tosatti E. On the nature of surface roughness with application to contact mechanics, sealing, rubber friction and adhesion. Journal of Physics: Condensed Matter 2004; 17:R1.

[7] Hoo Fatt MS, Ouyang X. Three-dimensional constitutive equations for Styrene Butadiene Rubber at high strain rates. Mechanics of Materials 2008; 40:1-16.

[8] Rouif S. Radiation cross-linked polymers: Recent developments and new applications. Nuclear Instruments and Methods in Physics Research Section B: Beam Interactions with Materials and Atoms 2005; 236:68-72.

[9] Xu C. The Self-Sealing Mechanism for Materials and Bonded Rings for Flange Joints. In: Digital Manufacturing and Automation (ICDMA), International Conference, 2010. p. 804-7.

[10] Khan AS, Baig M, Hamid S, Zhang H. Thermo-mechanical large deformation responses of Hydrogenated Nitrile Butadiene Rubber (HNBR): Experimental results. International Journal of Solids and Structures 2010; 47:2653-9.

[11] Tochizawa M, Inoue N, Tanaka M, Nishi Y. Self-sealing materials for space debris shield. in: Proceeding of the SPIE, 2004. p. 318-24.

[12] White SR, Sottos NR, Geubelle PH, Moore JS, Kessler MR, Sriram SR, et al. Autonomic healing of polymer composites. Nature 2001; 409:794-7.

[13] Moll JL, White SR, Sottos NR. A Self-sealing Fiber-reinforced Composite. Journal of Composite Materials 2010; 44:2573-85.

[14] Lee HXD, Wong HS, Buenfeld NR. Potential of superabsorbent polymer for self-sealing cracks in concrete. Advances in Applied Ceramics 2010; 109:296-302.

[15] Pang JWC, Bond IP. 'Bleeding composites'—damage detection and self-repair using a biomimetic approach. Composites Part A: Applied Science and Manufacturing 2005; 36:183-8.

[16] Kessler MR, Sottos NR, White SR. Self-healing structural composite materials. Composites Part A: Applied Science and Manufacturing 2003; 34:743-53.

[17] Heimbs S, Van Den Broucke B, Duplessis Kergomard Y, Dau F, Malherbe B. Rubber Impact on 3D Textile Composites. Applied Composite Materials 2012; 19:275-95.

[18] Mines R, McKown S, Birch R. Impact of aircraft rubber tyre fragments on aluminium alloy plates: I—Experimental. International Journal of Impact Engineering 2007; 34:627-46.

[19] Karagiozova D, Mines R. Impact of aircraft rubber tyre fragments on aluminium alloy plates: II—Numerical simulation using LS-DYNA. International Journal of Impact Engineering 2007; 34:647-67.

[20] Toso-Pentecôte N, Johnson A, Chabrier G. Modelling and simulation of tyre impacts on stiffened composite panels. Composites 2009; 2:1-3.

[21] Neves R, Micheli G, Alves M. An experimental and numerical investigation on tyre impact. International Journal of Impact Engineering 2010; 37:685-93.

[22] Mooney M. A theory of large elastic deformation. Journal of Applied Physics 1940; 11:582-92.

[23] Jia X, Huang Z, Zu X, Gu X, Zhu C, Zhang Z. Experimental study on the performance of woven fabric rubber composite armor subjected to shaped charge jet impact. International Journal of Impact Engineering 2013; 57: 134-144.

[24] Jia X, Huang Z, Guo M, Zu X, Ji L. Study on impact response of laminated woven fabric rubber composite armour against shaped charge jet. Plastics, Rubber and Composites 2015; 44:351-361.

[25] Jia X, Huang Z, Zu X, Xiao Q. Theoretical and Experimental Study on the Effects ofImpact Angle on the Performance of Kevlar Woven Fabric Rubber Composite Armor against Shaped Charge Jet Impact. Propellants, Explosives, Pyrotechnics 2015; 40:945-953.

[26] Ogden RW. Large Deformation Isotropic Elasticity - On the Correlation of Theory and Experiment for Incompressible Rubberlike Solids Proceedings of the Royal Society of London A Mathematical and Physical Sciences 1972; 326:565-84.

[27] ANSYS AUTODYN version 11.0 what is new? <http://www.ewp.rpi.edu/hartford/~ernesto/F2010/EP1/Materials4Students/Danyluk/autodyn-new-features.pdf>.

[28] Roland CM, Fragiadakis D, Gamache RM. Elastomer-steel laminate armor. Composite Structures 2010; 92:1059-64.

[29] Cai, L, Al-Ostaz, A, Li, X, Fowler, C, Cheng, A. H. D, & Alkhateb, H. Protection of steel railcar tank containing liquid chlorine from high speed impact by using polyhedral oligomeric silsesquioxane-enhanced polyurea. International Journal of Impact Engineering 2015; 75, 1-10.

[30] Backman ME, Goldsmith W. The mechanics of penetration of projectiles into targets. International Journal of Engineering Science 1978; 16:1-99.

[31] Xue L, Mock Jr W, Belytschko T. Penetration of DH-36 steel plates with and without polyurea coating. Mechanics of Materials 2010; 42:981-1003.

[32] Børvik T, Dey S, Clausen AH. Perforation resistance of five different high-strength steel plates subjected to small-arms projectiles. International Journal of Impact Engineering 2009; 36:948-64.

[33] Børvik T, Hopperstad OS, Berstad T, Langseth M. A computational model of viscoplasticity and ductile damage for impact and penetration. European Journal of Mechanics - A/Solids 2001; 20:685-712.

[34] Dey S, Børvik T, Hopperstad OS, Leinum JR, Langseth M. The effect of target strength on the perforation of steel plates using three different projectile nose shapes. International Journal of Impact Engineering 2004; 30:1005-38.

[35] Likozar B, Krajnc M. A study of heat transfer during molding of elastomers. Chemical Engineering Science 2008; 63:3181-92.

[36] Hayhurst CJ, Clegg RA. Cylindrically symmetric SPH simulations of hypervelocity impacts on thin plates. International Journal of Impact Engineering 1997; 20:337-48.

[37] Chen EP. Numerical simulation of penetration of aluminum targets by spherical-nose steel rods. Theoretical and Applied Fracture Mechanics 1995; 22:159-164.